Simulation of Human Interaction with Mobile Telephones Using Hybrid Techniques Over Coupled Domains

Mohab A. Mangoud, Raed A. Abd-Alhameed, and Peter S. Excell, *Senior Member, IEEE*

***Abstract*—An approach to hybridization of the method of moments and the finite-difference time-domain method is investigated in this paper. This hybrid method is capable of analyzing a system of multiple discrete regions by employing the principle of equivalent sources to excite their coupling surfaces. The case of multiple sources in the presence of scattering objects is discussed. To develop the approach and test its validity, some examples are given using the same numerical method in multiple regions: the results compare well with other available data. The theory of the heterogeneous hybrid method is then developed and validated. It is shown that this technique has the great advantage of accurately modeling complex and arbitrarily oriented mobile telephone handset antennas in the proximity of a detailed voxel representation of the human head, as required for safety and radiation pattern assessments.**

***Index Terms*—Bioelectromagnetics, computational electromagnetics, finite-difference time-domain method, hybrid methods, method of moments, mobile telephones, safety.**

I. Introduction

THE frequency-domain method of moments (MoM) and finite-difference time-domain (FDTD) method are widely used for analyzing complex electromagnetic problems. Treating electrically large and/or penetrable structures with the MoM requires extensive computational resources, while accurate models of wire and curved structures are difficult to implement in the FDTD method. A hybrid method was thus developed that allows efficient analysis of situations involving such structure combinations. Hybrid methods operating entirely in the time domain have been reported in the literature [1], [2], but the time-domain MoM is not at the state of maturity and flexibility of the frequency-domain version. Thus, this paper ultimately addresses the problem of hybridization of the FDTD method with the frequency-domain MoM—both familiar "industry standard" techniques. The problem is divided into separate regions, each of which may be modeled by the most suitable method (e.g. MoM for man-made devices, FDTD for biological tissues). The coupling between regions is accounted for by employing the equivalence principle on the bounding surfaces.

To test the concept, the authors' frequency-domain version of the MoM [3], [4] was used. This employs Galerkin's solution with polynomial basis functions in the analysis of structures consisting of wires, strips, and conducting surfaces of arbitrary shape, combined with small regions of inhomogeneous dielectric. It is, however, also possible to interface with industry-standard codes such as the Numerical Electromagnetics Code (NEC) [5], [6]. The number of iterations required for the solution to converge was investigated, as this could have a crucial effect on the viability.

Manuscript received November 24, 2000; revised May 3, 2000.

The authors are with the Telecommunications Research Centre, University of Bradford, Brandford BD7 1DP, U.K.

Publisher Item Identifier S 0018-9480(00)09693-9.

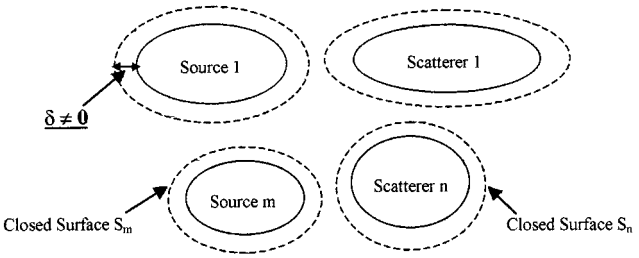

Fig. 1. Basic structure of the problem.

II. Validation and Testing of the Hybrid Technique

As a first step in developing the technique, the same computational electromagnetics (CEM) formulation was applied in separate regions, linked via equivalence-principle surfaces. After the techniques had been developed and proven, heterogeneous sets of formulations were investigated.

A. MoM in Two Regions

Consider the geometry of the problem given in Fig. 1. The geometry can be subdivided into n regions provided there are no physical attachments between them. Each region can be represented as a source or scatterer. Since the problem space is divided into n regions, n subdomains can be created by introducing closed surfaces S_i (for $i = 1, \ldots, n$), enclosing each region. Each subdomain can then be treated separately as follows.

Initially, each source region is solved (using a preferred CEM method) for the induced current, assuming the region to be in free space. The induced currents in that particular region are used to evaluate the fields on the enclosing surface. The fields due to all source regions are then used as excitation sources for the scattering due to all of the regions. The induced currents in each scatterer region are used to compute the back-scattered fields on the closed surface surrounding that region.

The effect of the back-scattered fields on a region containing a source was accounted for as impressed excitation fields in the source region. The new induced currents in this source region

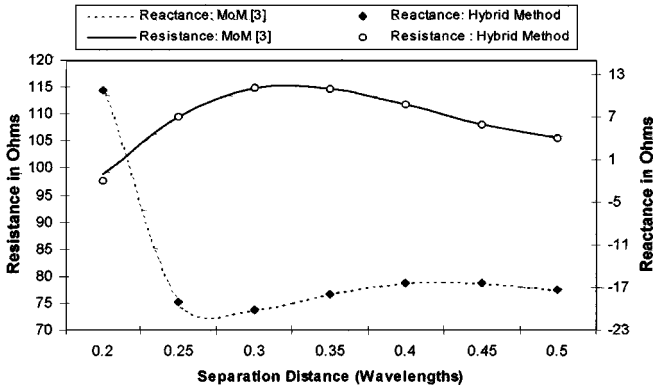

Fig. 2. Input impedance of 0.47λ dipole adjacent to a slab of simulated human brain material (MoM/MoM coupled regions and single MoM treatment [3]).

were used to obtain excitation fields in all other source and scatterer regions. Scatterer regions were dealt with in the same way. An iterative procedure was then used to obtain convergence of the results for the interaction between the regions. This multiple reaction iteration scheme can be stated in mathematical form, taking as an example, the MoM expression for the current in terms of the induced electrical currents. The induced currents in the region p at the ith iteration are given by

$$\mathbf{J}_p^i = -\langle \mathbf{J}_{tp} \cdot \mathbf{E}_{tp} \rangle^{-1} \sum_{k \neq p}^{n} \langle \mathbf{J}_{tp} \cdot \mathbf{E}_{tk} \rangle \mathbf{J}_k^{i-1} + \mathbf{J}_{p\text{free}} \qquad (1)$$

where $\mathbf{J}_{p\text{free}}$ is the free-space current of region p. This current is zero if this region is considered to be a scatterer region. $\mathbf{J}_{tp}$ is the current test function on region p, $\mathbf{E}_{tp}$ is the scattered field due to the test function $\mathbf{J}_{tp}$, $\mathbf{E}_{tk}$ is the field due to the test function $\mathbf{J}_{tk}$, $\mathbf{J}_k$ is the induced current in region k, i is the iteration number, and $\langle \mathbf{A} \cdot \mathbf{B} \rangle$ is the inner product of $\mathbf{A}$ and $\mathbf{B}$. The second inner product of (1) is the excitation vector due to the region k.

The current $\mathbf{J}_p$, due to the fields on the surface enclosing region k, can be expressed as follows:

$$\mathbf{J}_p^i = -\langle \mathbf{J}_{tp} \cdot \mathbf{E}_{tp} \rangle^{-1} \sum_{k \neq p}^{n} \langle \mathbf{J}_{tp} \cdot \mathbf{E}_{tk}(\mathbf{J}_{sk}, \mathbf{M}_{sk}) \rangle + \mathbf{J}_{p\text{free}} \quad (2)$$

where $\mathbf{J}_{sk}$ and $\mathbf{M}_{sk}$ are the equivalent electric and magnetic currents on the surface k.

Two examples may be used to test the method:

Example 1: Fig. 2 shows the input impedance of a dipole of length 0.47λ and radius 0.0045λ, located adjacent to a slab of simulated human brain material, for different distances between their centers. The slab has dimensions $0.25\lambda \times 0.0625\lambda \times 0.5\lambda$, relative permittivity 41.3 and conductivity 0.83 Sm^{-1}. The results of the hybrid method, using two separate coupled MoM regions, are in excellent agreement with results using a single MoM region [3].

Example 2: Three parallel dipoles of length 0.47λ and radius 0.0045λ were considered in order to test the validity of the hybrid method with multiple sources (Fig. 3). Each of them was treated as being within a separate domain and two of them were excited by delta source generators of amplitude $(1 + j0)$ V. The input impedances versus the number of iterations are shown in Figs. 4 and 5. Rapid convergence is observed within

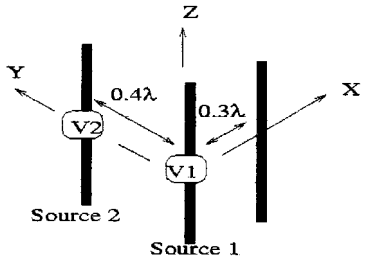

Fig. 3. Antenna geometry of MoM/MoM Example 2.

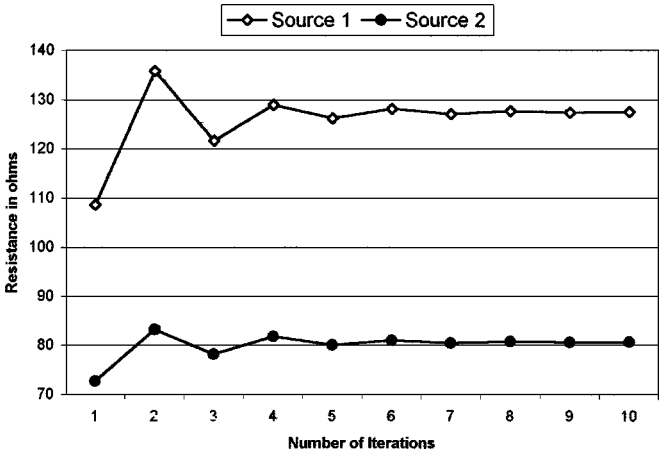

Fig. 4. Input resistance of the source dipoles in Fig. 3.

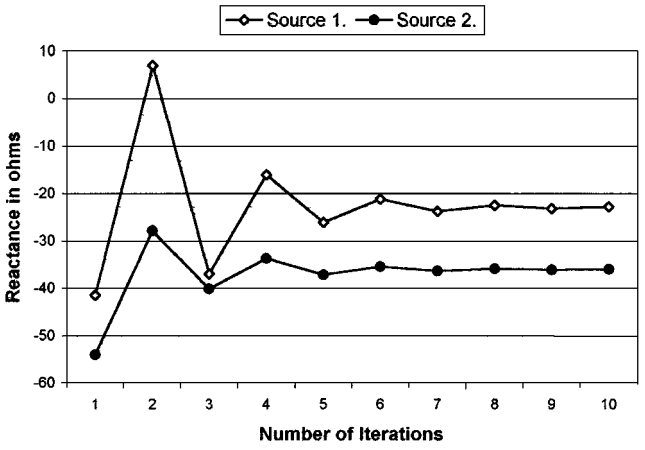

Fig. 5. Input reactance of the source dipoles in Fig. 3.

a few iterations. The impedances obtained were $128 - j23\ \Omega$ and $81 - j36\ \Omega$ for Sources 1 and 2 respectively. A separate (single region) MoM model of the system was also run, giving corresponding impedances of $127 - j22\ \Omega$ and $80 - j35\ \Omega$, thus confirming the accuracy of the two-region result.

III. Heterogeneous Hybrid (MoM/FDTD) Technique

Fig. 6 shows an outline diagram of the iteration flow-chart for the proposed MoM/FDTD hybrid method. In this method, the frequency-domain version of the MoM is used and, hence, simple Fourier transforms (including phase information) have to be applied between each iterative step. The source and scatterer are located in two separate regions. The induced currents for the source region are obtained, excluding the effect of the

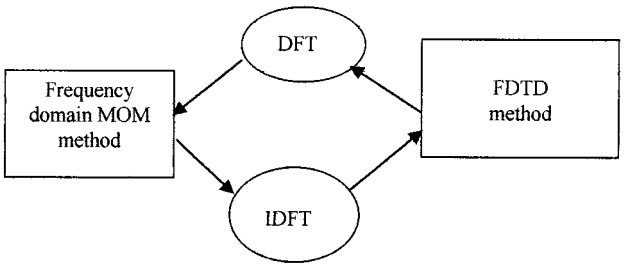

Fig. 6. Iteration flow-chart for MoM/FDTD model.

scatterer, using the frequency-domain version of the MoM. The fields due to these currents are obtained on the closed surface (Huygens surface) [7] that separates the source from the scatterer. Oscillating with respect to a reference phase of the source, these fields or their equivalent surface currents are converted to time-domain excitation incident fields or current sources using an inverse discrete Fourier transform. The FDTD algorithm is now executed with these time-domain sources to obtain the induced currents on the scatterer. The back-scattered fields on the source side of the Huygens surface are considered to be the excitation sources for the source region. These fields or their equivalent current sources are transferred to the frequency domain using a discrete Fourier transform, in which the phase difference relative to the reference phase of the source is taken into account. The MoM is then used in reverse to evaluate the induced currents on the source region due to both the source excitation region and the induced equivalent-current sources from the FDTD method. The method is repeated until a steady-state solution is obtained.

A. Theory of the Method

Firstly, consider Fig. 7, which shows (as a general example) two source regions (1 and 2) and one scatterer region. The source regions are bounded by the equivalence-principle closed surfaces S_{ci} ($i = 1, 2$). The method starts by applying the MoM for each source separately (assuming internal excitation exists in each source region). The fields on the equivalence-principle surfaces S_{ci} can then be computed using the previously calculated currents in each region. Thus, the excitation surface currents that are required to run the FDTD, including the scatterer region, can be evaluated as follows:

$$\mathbf{M}_{si} = \hat{\mathbf{n}}_i \times \mathbf{E}_{si}(\mathrm{S}_{ci}) \tag{3}$$

$$\mathbf{J}_{si} = \hat{\mathbf{n}}_i \times \mathbf{H}_{si}(\mathrm{S}_{ci}) \tag{4}$$

where $\mathbf{E}_{si}$ and $\mathbf{H}_{si}$ (for $i = 1, 2$) are the scattered electric and magnetic fields on the equivalence-principle surfaces S_{ci} ($i = 1, 2$), respectively. $\mathbf{J}_{si}$ and $\mathbf{M}_{si}$ are the equivalent surface currents on the equivalence-principle surfaces S_{ci}, respectively. $\hat{\mathbf{n}}_i$ is the ith unit vector directed outwards from the ith closed-surface S_{ci}.

Thus, these currents are treated as the source in the FDTD domain, propagating fields to the scatterer by using the E and H time-domain equations. The scattered regions are considered to be inside each of the equivalent closed surfaces shown in Fig. 7, whereas the total fields are considered to be exterior to

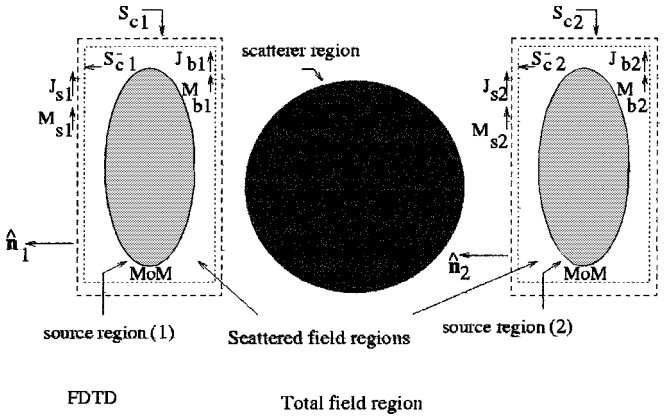

Fig. 7. Basic structure of the hybrid MoM/FDTD formulation in multiple regions.

the equivalent surfaces (other configurations of the surfaces are possible: those which minimize the size of the Huygens surface are normally the most efficient). Thus, the time-domain equations on the surfaces S_{ci} (for $i = 1, 2$) can be stated as follows:

$$\nabla \times \mathbf{E} = -\frac{\partial \mathbf{B}}{\partial t} - \mathbf{M}_{is} \tag{5}$$

$$\nabla \times \mathbf{H} = \frac{\partial \mathbf{D}}{\partial t} + \mathbf{J}_{is}. \tag{6}$$

The resulting difference equations for the electric- and magnetic-field components, based on (5) and (6), are given in [8] by applying the total-field/scattered-field formulation. The back-scattered fields for each source region were computed by FDTD at S_{ic}^{-} (ith closed-surface interior to the surface S_{ci} and bounding the ith source region). These fields for the ith source region include the effect of the scatterer and source region j (where $j \neq i$) and, hence, each source region will be treated separately to determine the new current distributions using the MoM as follows.

The ith equivalent surface currents due to these fields that represent an additional source to the MoM domain are given by

$$\mathbf{M}_{bi} = \hat{\mathbf{n}}_i \times \mathbf{E}_{bi}(\mathbf{S}_{ci}^{-}) \tag{7}$$

$$\mathbf{J}_{bi} = \hat{\mathbf{n}}_i \times \mathbf{H}_{bi}(\mathbf{S}_{ci}^{-}) \tag{8}$$

where $\mathbf{E}_{bi}$ and $\mathbf{H}_{bi}$ (for $i = 1, 2$) are the back-scattered electric and magnetic fields on the equivalent surfaces S_{ci}^{-} ($i = 1, 2$), respectively. $\mathbf{J}_{bi}$ and $\mathbf{M}_{bi}$ are the equivalent surface currents on the equivalent surfaces S_{ci}^{-} ($i = 1, 2$), respectively.

Now, the voltage back-scattered (the excitation for the MoM) on the ith source region can be evaluated using the reciprocity theorem

$$V_{bi} = \int_{S_{ci}^{-}} (\mathbf{E}_{ti} \cdot \mathbf{J}_{bi} - \mathbf{H}_{ti} \cdot \mathbf{M}_{bi})\, ds_{ci}^{-}, \qquad \text{for } i = 1, 2 \tag{9}$$

where $\mathbf{E}_{ti}$ and $\mathbf{H}_{ti}$ are the electric and magnetic test fields of the ith source region. If the cell meshing used in the FDTD region is very small compared with the operating wavelength, (9) can

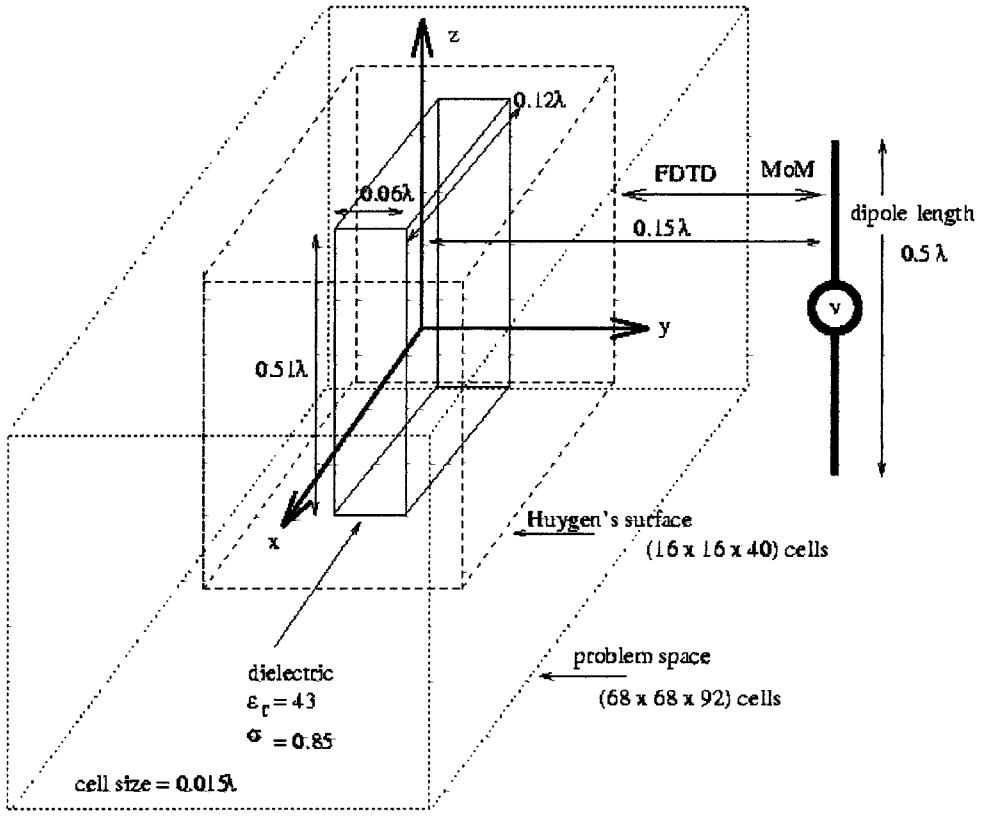

Fig. 8. Model used to test the hybrid MoM/FDTD method: a dipole adjacent to a thin dielectric slab.

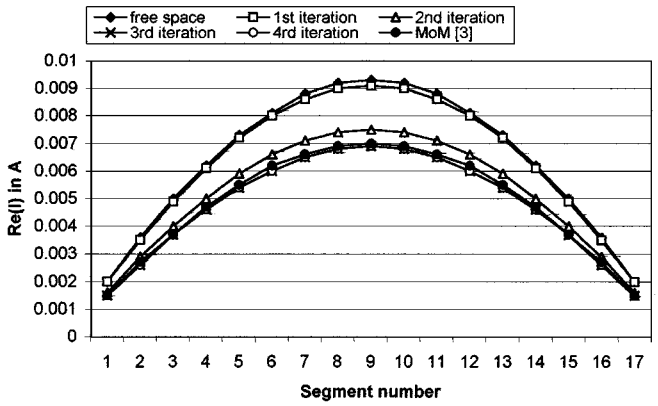

Fig. 9. Convergence of the real part of the total current along the dipole versus segment number compared with a pure-MoM solution for the same problem [3] and a pure-MoM model of the dipole in free space.

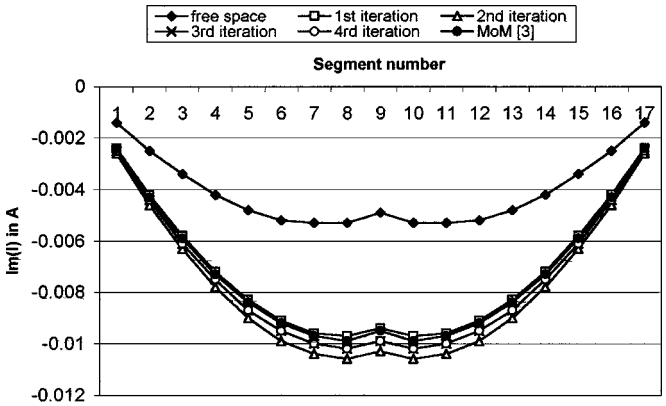

Fig. 10. Convergence of the imaginary part of the total current along the dipole versus segment number (with comparisons as in Fig. 9).

be simplified and discretized by changing the surface integral to summation over the cell outer surfaces and evaluating the voltage back-scattered, corresponding to the center of the cell surface; thus,

$$V_{bi} = \sum_{u_{s_{ci}^-}} \Big(\mathbf{E}_{ti}(\mathbf{r}, \mathbf{r}'_{ni}) \cdot \mathbf{J}_{bi_n} - \mathbf{H}_{ti}(\mathbf{r}, \mathbf{r}'_{ni}) \cdot \mathbf{M}_{bi_n}\Big)\mathbf{a}_n, \quad \text{for } i = 1, 2 \tag{10}$$

where $\mathbf{r}'_{ni}$ is the ith position vector of the center of the cell surface S_{ci}^-, $n_{s_{ci}}$ is the total number of the cell surfaces on the ith equivalent surface S_{ci}^-, and a_n is the surface area of the cell.Therefore, $\mathbf{J}_{bi_n}$ and $\mathbf{M}_{bi_n}$ are considered to be the ith equivalent surface currents at the center of the cell surface n of the equivalent closed surface S_{ci}^-. Since the excitation voltages of each source region are known, the MoM can be executed to compute the new currents (for each source region) and the procedure can be repeated until the steady-state solution is reached.

B. Results

Several examples were simulated as follows to test the proposed method.

Example 1: In this example, the field induced in a thin slab of simulated brain material was studied; the slab had dimensions

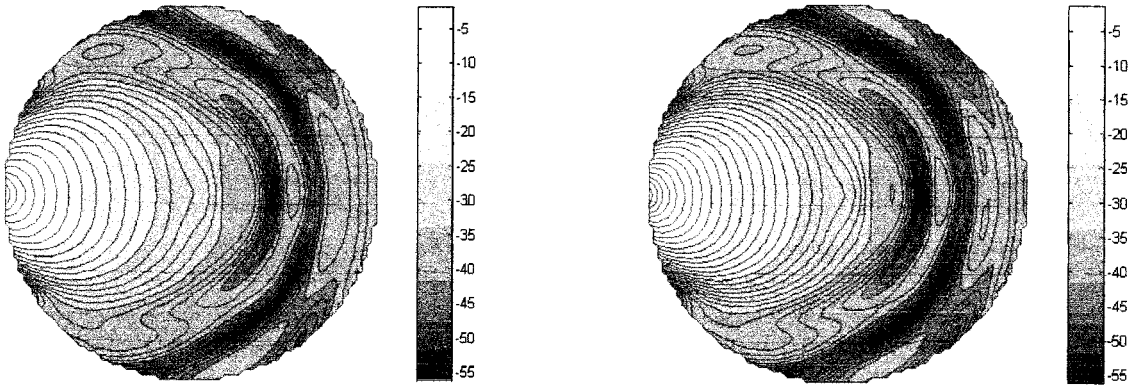

(a) (b)

Fig. 11. Computed SAR distribution in a plane through the center of a sphere adjacent to a dipole (SAR expressed in dB, normalized to the maximum SAR) (a) Hybrid MoM/FDTD (max. SAR, normalized to 1 W radiated $= 14.5$ dB). (b) Pure FDTD (max. SAR, normalized to 1 W radiated $= 15.6$ dB).

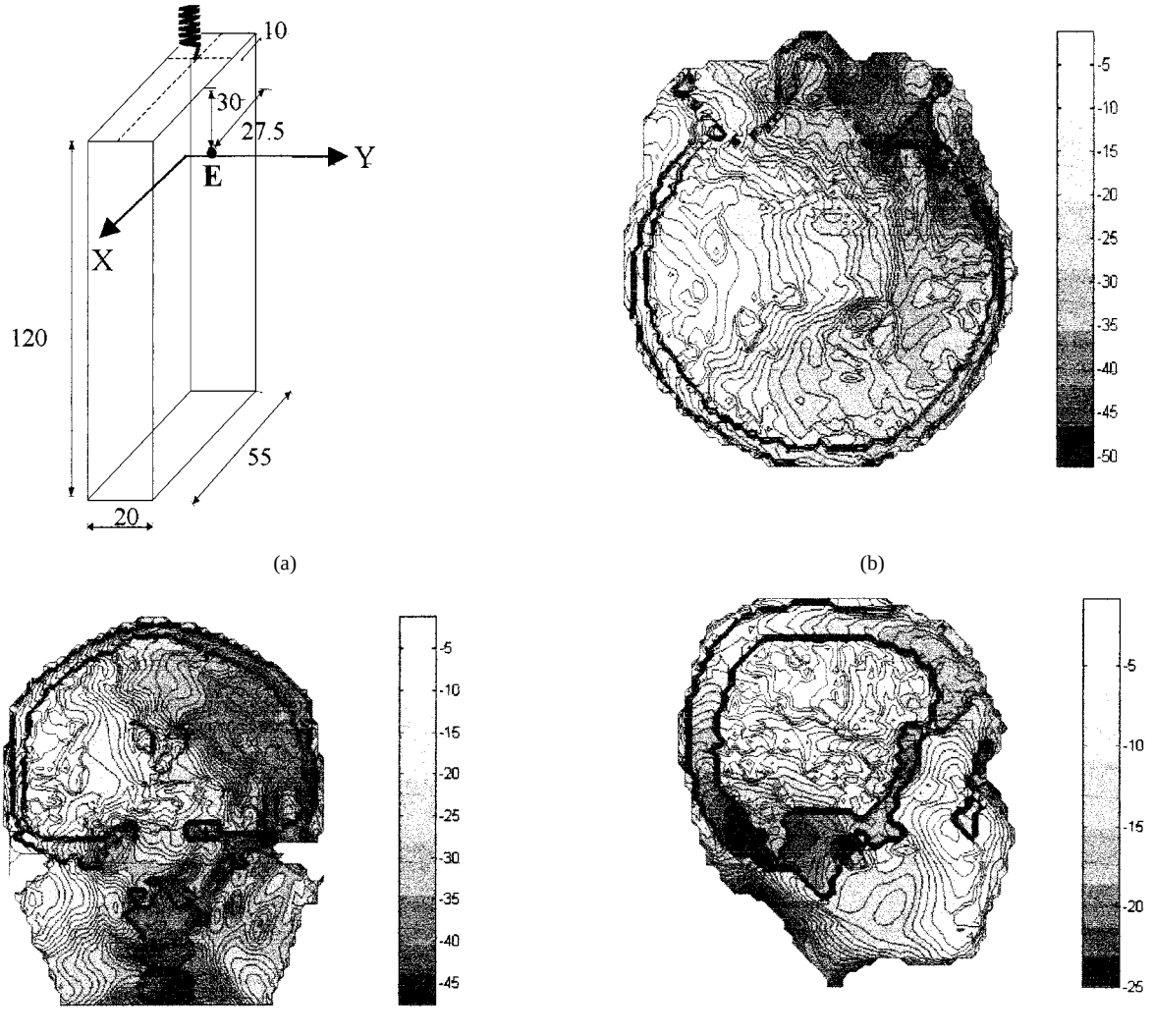

(a) (b)

(c) (d)

Fig. 12. (a) Geometry of the 1710-MHz helical antenna on a metal box simulating a handset (dimensions in mm). (b) SAR distribution (normalized to maximum SAR) over horizontal x–y-plane of the realistic head through the maximum SAR point, adjacent to helical antenna handset rotated by 30°. (c) As (b), for vertical y-z plane. (d) As (b), for vertical x–z-plane within head, 2.5 cm from side nearest to handset.

$0.12\lambda \times 0.06\lambda \times 0.51\lambda$ and was inserted into the scatterer region. As shown in Fig. 8, the separation distance between the dipole and dielectric was chosen to be 0.15λ. Figs. 9 and 10 show that the solution for the real and imaginary parts of the total current along the wire antenna converges in four iterations of the hybrid method. Also, the figures show standard single-do-

main MoM solutions for the current distribution when the dipole is in free space and when the dielectric is included [3]. Good agreement between the results of the two methods is observed, taking account of the very different treatments used to represent the dielectric. The geometrical configuration chosen for this example was such that the scatterer region, modeled by FDTD, was a sub-domain within a larger MoM region. For situations involving coupling between a small source and a relatively large dielectric mass (e.g., between a mobile telephone and the human head) the most efficient strategy is to make the MoM source region a sub-domain within the scatterer's FDTD region. This minimizes the size of the Huygens surface and, hence, minimizes the computational task.

Example 2: A half-wavelength dipole antenna of radius 1 mm was modeled using the MoM at an operating frequency of 900 MHz. This was placed within an equivalent Huygens surface of size $10 \times 10 \times 70$ cells, modeled inside the FDTD problem space, which was of size $138 \times 112 \times 112$ cells with a cell size of 2.5 mm. A biological sphere of radius 20 cm was modeled with the following electrical properties: $\varepsilon_r = 56.4$, $\sigma = 1.1$ S/m, $\rho = 1050$ kg/m^3. The distance between the sphere and the dipole was 0.5 cm. The perfectly matched layer (PML) absorbing boundary condition (ABC) [9] was used, with a thickness of six cells. The specific absorption rate (SAR) distribution calculated using the hybrid method is given in Fig. 11(a), which is in excellent agreement with the result of a homogeneous FDTD simulation, shown in Fig. 11(b): in the FDTD model, the same cell size was used with a dipole feeding gap of 2.5 mm. Using the hybrid method, and normalizing to 1 W radiated from the dipole, the power absorbed in the biological sphere was found to be 734.24 mW, the maximum SAR in any cell was 28.93 W/kg, and the maximum SARs averaged over 10 and 1 g were 9.443 and 15.43 W/kg, respectively. The input impedance of the dipole changed from $98 + j39\ \Omega$ to $59 + j14\ \Omega$ in the presence of the sphere. The hybrid method converged after three iterations: the maximum SAR found after the first iteration was 29.57 W/kg, which is only 2.2% different from that of the third iteration.

Example 3: A normal-mode helical antenna mounted on the top corner of a metal handset box was investigated in the presence of a realistic head image, taken from a magnetic resonance imaging (MRI) scan of a real human head. The image has a resolution of $0.909 \times 0.909 \times 1.480$ mm and is segmented into 13 different tissue types [10].

Fig. 12(a) shows the geometry of the MoM-modeled handset: point E corresponds to the projection of the ear canal on to the metal box. The helical antenna, having 5.2 turns, is modeled by using curved segmentations [4] and it was driven at 1710 MHz by a delta-gap generator at its base. The wire radius is 0.4 mm and radius of the helix and pitch distance are 2 and 2.5 mm, respectively. The dimensions of the box are 120 mm $\times$ 55 mm $\times$ 20 mm and it is located 5 mm from the head such that the local horizontal axis (ear to ear) of the head is 30 mm below the top surface of the box. The distribution of the SAR in orthogonal slices of the head for the case where the handset is rotated by 30° is shown in Fig. 12(b)–(d). The rotation is about the x-axis in Fig. 12(a) and is in such a direction as to bring the handset into a "natural" pose: it would be virtually impossible to model such a helical antenna in this pose using pure FDTD. The near fields of the helical antenna handset, computed without the head, but retaining the FDTD region as free space, are presented in Fig. 13, where E_z is displayed versus the distance in the z-direction at distances of 1.5, 2, and 2.5 cm, respectively, in the y-direction, at $x = 0$. Very good agreement with the industry-standard program NEC [5] is obtained. The radiation patterns for a vertically positioned helical antenna handset, obtained using a frequency-domain near- to far-field transformation of the hybrid method, with and without the head, are shown in Fig. 14.

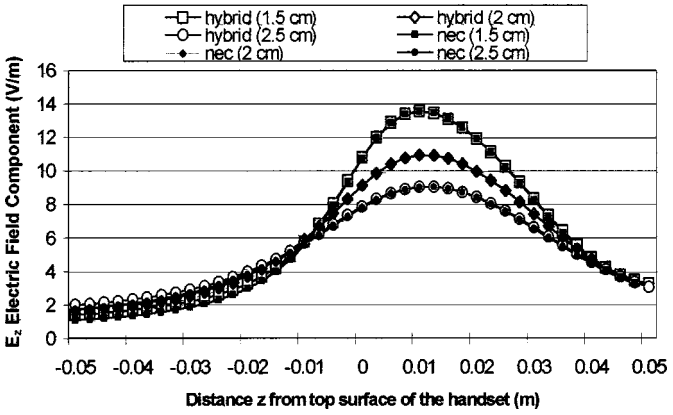

Fig. 13. Near-field E_z distribution along the z-axis at $x = 0$, $y = 1.5, 2$, and 3 cm for the helical antenna handset in free space, using the hybrid MoM/FDTD method (head region represented as free space), and compared with NEC [5].

IV. Conclusions

The hybrid treatments of the electromagnetic behavior of coupled multiple regions using both homogeneous and heterogeneous CEM formulations have provided stable and accurate results. The results of test cases were in excellent agreement with published results and physical expectations. The number of iterations required to account for the multiple reactions between regions was investigated: rapid convergence was found for structures consisting of two or more regions.

The method is particularly useful for analyzing complex problems involving coupling between antennas and dielectric volumes, especially biological tissue. This is because it permits the computationally efficient FDTD method to be used for the dielectric, but the MoM, which represents conducting structures more accurately, for the antenna. Thus, it can be concluded that the hybrid MoM/FDTD technique is very good for safety assessment and field simulations of arbitrarily oriented mobile telephones using helical antennas, as are increasingly being used as the main antenna in commercial mobile telephone handsets.

Depending on the problem investigated, it appears that, in general, only two or three iterations are required for convergence and it would appear that five might be expected to be a realistic maximum. Thus, bearing in mind the need to run two different models and handle the coupling between them, the computational cost of the hybrid technique is roughly between four and ten times that of a comparable FDTD simulation that uses the same cell size: this is normally within the capability of

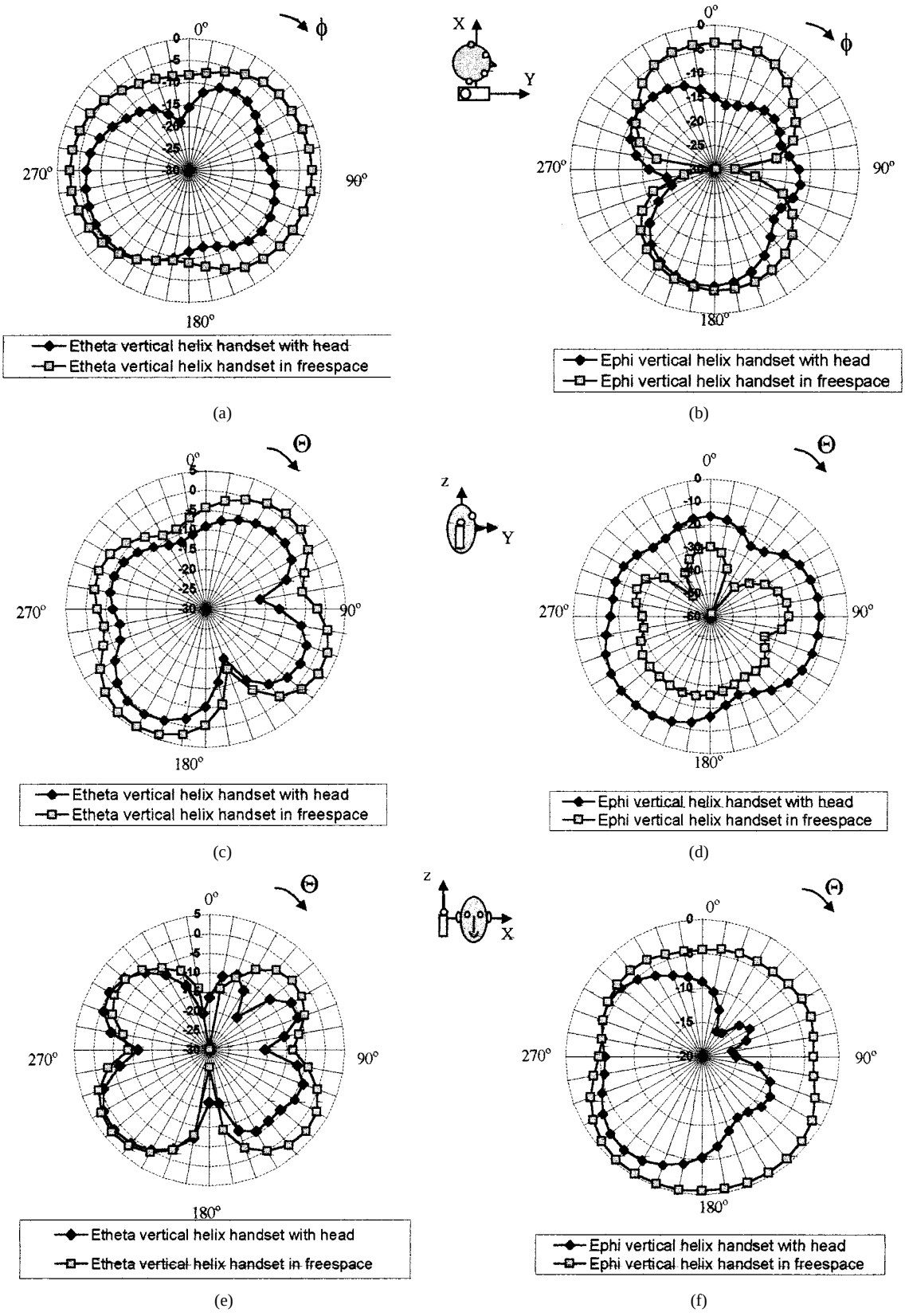

Fig. 14. E_θ and E_ϕ far-field components in decibels for vertically oriented helical antenna handset with and without realistic head. Scale: dBV/m normalized to 1-m distance with 1-V drive to antenna. (a) Azimuth patterns ($\theta = 90°$). (b) Azimuth patterns ($\theta = 90°$). (c) Elevation patterns ($\phi = 90°$). (d) Elevation patterns ($\phi = 90°$). (e) Elevation patterns ($\phi = 0°$). (f) Elevation patterns ($\phi = 0°$).

modern computers. On the other hand, the hybrid method is able to model problems with curved arbitrarily oriented structures in the vicinity of inhomogeneous materials, which is not possible with any other method.

ACKNOWLEDGMENT

The authors wish to thank J. A. Vaul, Electronic and Electrical Engineering Department, University of Bradford, Bradford, U.K., for his help and expertise in FDTD.

REFERENCES

[1] A. R. Bretones, R. Mittra, and G. Martin, "A hybrid technique combining the MoM in the time domain and FDTD," *IEEE Microwave Guided Wave Lett.*, vol. 8, pp. 281–283, Aug. 1998.

[2] G. Cerri and P. Russo *et al.*, "MoM-FDTD hybrid technique for analyzing scattering problems," *Electron. Lett.*, vol. 34, pp. 433–440, 1998.

[3] R. A. Abd-Alhameed and P. S. Excell, "Analysis of dielectrically-loaded wire, strip and patch antennas using the method of moments," in *Proc. IEE Comput. Electromag. Conf.*, Bath, U.K., 1996, pp. 306–311.

[4] ——, "Analysis of a normal-mode helical antenna including nonuniform wire surface current effects," *Proc. Inst. Elect. Eng.*, vol. 146, no. 1, pp. 1–5, 1999.

[5] G. J. Burke and A. J. Poggio, "Numerical electromagnetics code (NEC): Method of moments," U.S. Naval Ocean Syst. Center, San Diego, CA, Rep. TD116, 1981.

[6] M. A. Mangoud, R. A. Abd-Alhameed, P. S. Excell, and J. A. Vaul, "Conduction current crossing domain boundaries in heterogeneous hybrid computational electromagnetics," *Electron. Lett.*, vol. 35, pp. 1786–1787, 1999.

[7] D. E. Merewether, R. Fisher, and F. W. Smith, "On implementing a numerical Huygens source scheme in a finite difference program to illuminate scattering bodies," *IEEE Trans. Nucl. Sci.*, vol. NS-27, pp. 1829–1833, June 1980.

[8] A. Taflove, *Computational Electrodynamics: The Finite Difference Time Domain Method*. Norwood, MA: Artech House, 1995.

[9] J. P. Berenger, "A perfectly matched layer for the absorption of electromagnetic waves," *J. Comput. Phys.*, vol. 4, pp. 185–200, 1994.

[10] P. S. Excell, "Computer modeling of high frequency electromagnetic field penetration into the human head," *Meas. Control*, vol. 31, no. 6, pp. 170–175, 1998.

Mohab A. Mangoud was born in Alexandria, Egypt, in 1971. He received the B.Sc. and M.Sc. degrees in electrical engineering from Alexandria University, Alexandria, Egypt, in 1993 and 1996, respectively, and is currently working toward the Ph.D. degree at the University of Bradford, Bradford, U.K.

Since 1993, he has been a Lecturer at the Arab Academy for Science and Technology, Alexandria, Egypt. His research interests are in optical CDMA communication systems, antenna design, CEM, and RF dosimetry for safety investigations.

Raed A. Abd-Alhameed was born in Basra, Iraq, in 1959. He received the B.Sc. and M.Sc. degrees from Basra University, Basra, Iraq, in 1982 and 1985, respectively, and the Ph.D. degree from the University of Bradford, Bradford, U.K., in 1997, all in electrical engineering.

Since 1997 he has been a Post-Doctoral Research Assistant (Lecturer since May 2000) at the University of Bradford, where he specializes in CEM and nonlinear circuit simulation.

Peter S. Excell (M'80–SM'84) received the Ph.D. degree from Bradford University, Bradford, U.K., in 1980, for his research in electromagnetic hazards.

He has been with the University of Bradford since 1971, and is currently a Professor of applied electromagnetics and Deputy Director of the Telecommunications Research Centre. Since 1991, his research has involved the computation and measurement of electromagnetic fields in the human body, during which time he commenced a large-scale study of procedures for testing of mobile telephones. He was a partner in a recently completed pan-European project to standardize such procedures across Europe. His other research interests include antenna design, the use of parallel computers in CEM, and superconducting filters and antennas.

Dr. Excell is a Chartered Engineer and a Fellow of the Institution of Electrical Engineers (IEE), U.K.